2017 SNMMI Highlights Lecture: General Nuclear Medicine

Patrick M. Colletti, MD, University of Southern California, Los Angeles

From the Newsline Editor: The Highlights Lecture, presented at the closing session of each SNMMI Annual Meeting, was originated and presented for more than 30 years by Henry N. Wagner, Jr., MD. Beginning in 2010, the duties of summarizing selected significant presentations at the meeting were divided annually among 4 distinguished nuclear and molecular medicine subject matter experts. Each year Newsline publishes these lectures and selected images. The 2017 Highlights Lectures were delivered on June 14 at the SNMMI Annual Meeting in Denver, CO. In this issue we feature the lecture by Patrick M. Colletti, MD, a professor of Radiology, Medicine, Biokinesiology, and Pharmaceutical Sciences at the University of Southern California (Los Angeles), who spoke on highlights in general nuclear medicine. Note that in the following presentation summary, numerals in brackets represent abstract numbers as published in The Journal of Nuclear Medicine *(2017;58[suppl 1]).*

Chemistry is life—this is the underlying principle for much of the outstanding general nuclear medicine presentations at this year's SNMMI meeting. As in previous years, multiple investigators presented novel chemical constructs for promising radiopharmaceuticals.

This year, presentations elucidating methods for efficient ^{18}F labeling and imaging were notable. One example came from Kobayashi et al. from the Research Centre Nihon Medi-Physics Co., Ltd. (Chiba, Japan) and University Hospital Würzburg (Germany), who reported on "Novel functional renal imaging with ^{18}F-fluorodeoxysorbitol (^{18}F-FDS) PET" [521]. This tracer is made by simple reduction from ^{18}F-FDG. In rat models of acute renal failure and unilateral ureteral obstruction, the researchers demonstrated favorable kinetics for functional renal imaging (Fig. 1). Urine concentrations of ^{18}F-FDS were comparable to those with ^{99m}Tc-diethylenetriamine pentaacetic acid. Last year the same group showed that sorbitol urinary clearance was also closely correlated with inulin clearance. This year they presented results that suggest that the advantage of high spatial/temporal resolution and the simple production method for ^{18}F-FDS could improve both the diagnostic performance and availability of renal imaging. In the future this tracer might be helpful in identifying bacterial infections, among other applications.

Choi et al. from the Brigham and Women's Hospital/Dana-Farber Cancer Center, Harvard Medical School (Boston, MA), and Hanyang University College of Medicine (Seoul, Korea) [1200] asked "Is cholecystokinin (CCK) administration or delayed imaging necessary when bowel excretion does not occur but the gallbladder fills promptly?" [1200]. Preferential gallbladder filling without ^{99m}Tc-HIDA excretion into the small bowel up to 1 hour is occasionally seen after CCK pretreatment or in the fasting state. Although this is recognized as a normal variant, many nuclear medicine physicians choose to administer CCK or obtain delayed images to exclude the possibility of common bile duct obstruction.

Patrick M. Colletti, MD

This study included the records of 155 patients in whom the gallbladder was quickly visualized but the small bowel remained without tracer at 1 hour. The authors looked at time of gallbladder visualization and time to liver parenchymal clearing. They found prompt clearance of liver parenchymal activity in 142 patients (91.8%), with the remaining 13 having mild-to-moderately delayed clearance with or without initial decreased hepatic uptake. None of the 142 patients had any event attributable to common bile duct obstruction on follow-up, and all patients in the group of 13 had additional imaging, with no common bile duct–related issues in 11. The authors concluded that when hepatobiliary scintigraphy partially visualizes the gallbladder but not the small bowel "the probability of identifying clinically relevant common bile duct obstruction by additional imaging with CCK or delayed imaging is virtually zero in the acute clinical setting, if liver parenchymal clearance is prompt." They suggested that CCK or delayed imaging can be reserved for those with delayed liver clearance of >50% at 60 minutes, either visually or by parenchymal retention.

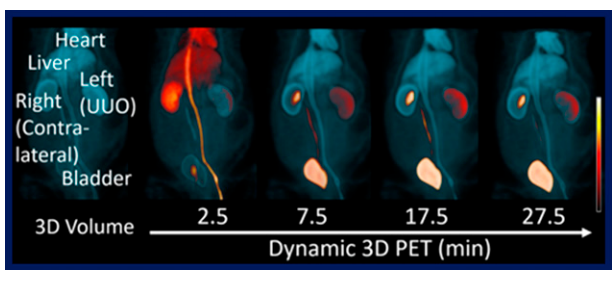

FIGURE 1. Dynamic 3D functional imaging with ^{18}F-fluorodeoxysorbitol (^{18}F-FDS) PET in a rat model of unilateral ureteral obstruction, acquired (left to right) 2.5, 7.5, 17.5, and 27.5 minutes after injection. The high spatial/temporal resolution and simple production method for ^{18}F-FDS could improve both the diagnostic performance and availability of renal imaging.

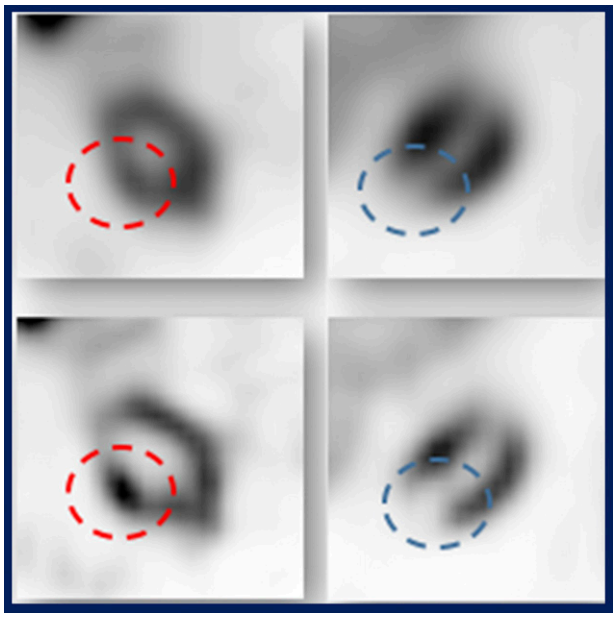

FIGURE 2. Quantitative SPECT/CT ^{99m}Tc-sestamibi renal imaging reconstructions (bottom) compared with those from the conventional Flash-3D algorithm (top) in hot (left, oncocytoma) and cold (right, renal cell carcinoma) masses.

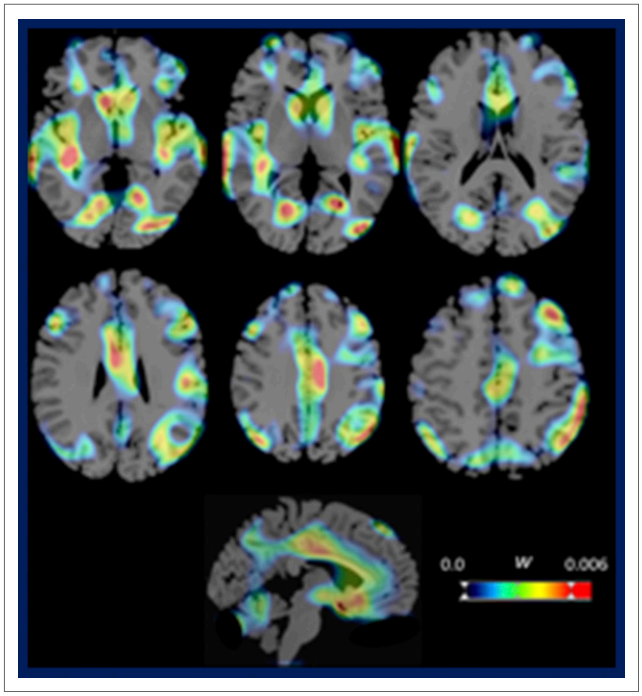

FIGURE 3. ^{18}F-FPEB PET imaging of metabotropic glutamate receptor subtype 5 (mGluR5) in alcohol dependence. A multivariate support vector machine was able to identify regions of decreased mGluR5 availability in the cortico-subcortical network in alcohol-dependent patients and separate out those whose dependency might be successfully treated from those in whom it might not.

Jones et al. from Johns Hopkins University and School of Medicine (Baltimore, MD) and the Universitatsklinikum Würzburg (Germany) reported on "Application of quantitative SPECT/CT reconstructions with ^{99m}Tc-sestamibi renal imaging of patients with cT1 renal masses" [745]. They have previously shown that relatively benign renal masses, such as oncocytomas, will take up sestamibi, whereas renal cell carcinoma does not. They have demonstrated this with both SPECT and planar imaging. In the study presented at this meeting, they showed that quantitative SPECT/CT (QSPECT), an emerging method that implements corrections for image-degrading factors that yield physically repeatable quantitative uptake in target and reference organs, is better able to differentiate lesions as "cold" or "hot" tumors. Figure 2 shows a comparison of conventional Flash 3D and the QSPECT technique in hot (oncocytoma) and cold (renal cell carcinoma) masses. The authors concluded that "this methodology will serve as a framework on which to build more robust quantitative biomarkers such as SPECT SUV" that "may provide more diagnostic certainty and improved classification of tumor subtypes to help guide patient management and avoid unnecessary surgeries." The possibility that someday surgeons will not be performing total or partial nephrectomies for benign lesions is encouraging.

Ceccarini et al. from University Hospitals Leuven–KU Leuven (Belgium) reported on "Accurate discrimination of alcoholic patients using a multivariate support vector machine (SVM) approach of metabotropic glutamate receptor subtype 5 (mGluR5) PET" [288]. The authors used ^{18}F-FPEB PET imaging to construct a voxel-based discriminative cerebral mGluR5 pattern for patients with alcohol dependence using an SVM approach to define the spatial discriminative features and identify individuals likely to respond to treatment from those likely to relapse. The study included 16 patients with a DSM-IV diagnosis of alcohol dependence and 32 age-matched healthy controls, all of whom underwent ^{18}F-FPEB PET imaging. The biodistribution visualized was similar to that seen with MR spectroscopy. However, with the addition of the SVM analysis the investigators were able to a identify regional decreased mGluR5 availability in the cortico-subcortical network in alcoholic patients (Fig. 3) and separate out fairly effectively those whose alcohol dependency might be successfully treated from those who might not respond to such treatment or might relapse. The authors pointed to the potential for personalized decision making in alcohol and other dependencies and called for additional studies to assess multivariate machine learning techniques to test the prognostic capacity of this approach for relapse propensity.

Watanabe et al. from Hokkaido University, Hokkaido University Graduate School of Medicine, and Hokkaido University Hospital (all in Sapporo, Japan) reported on "First-in-human study of ^{18}F-DiFA, an improved PET probe for tumor hypoxia, in 6 healthy volunteers" [839]. ^{18}F-DiFA is a new imaging tracer that targets tumor hypoxia, with the

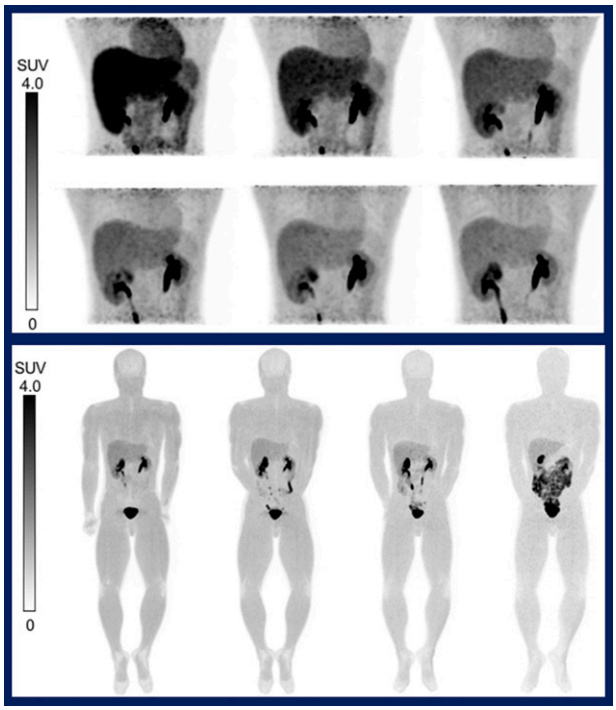

FIGURE 4. Top: Representative PET image of tracer biodistribution in a healthy volunteer (top, left to right) at 7–13, 14–21, and 22–28 minutes and (bottom, left to right) 29–36, 37–44, and 45–52 minutes after injection of 717.8 MBq ^{18}F-DiFA. Bottom: Representative PET images of uptake at (left to right) 1, 2, 4, and 6 hours after injection. ^{18}F-DiFA targets tumor hypoxia, with the potential to overcome some of the timing disadvantages of ^{18}F-fluoromisonidazole, with lower lipophilicity and easier radiosynthesis.

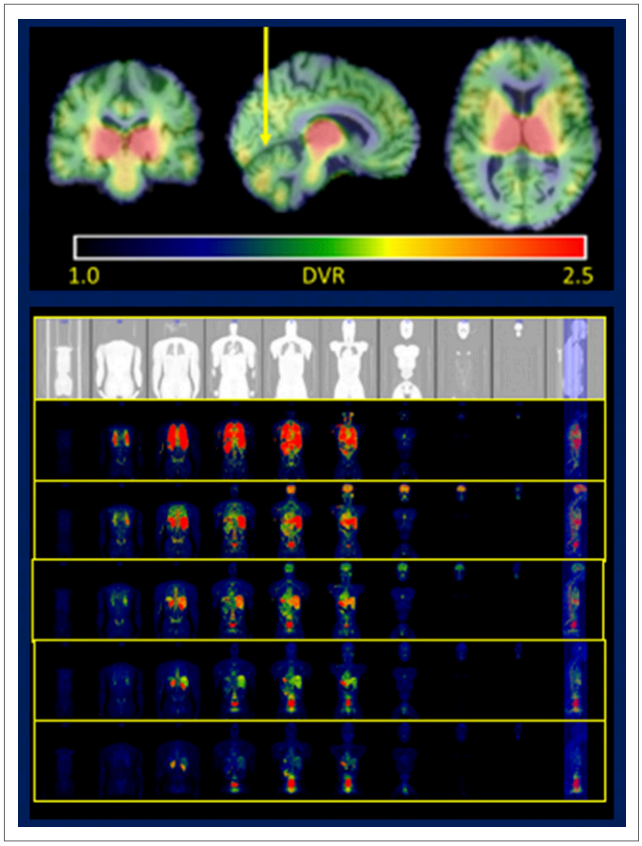

FIGURE 5. ^{18}F-nifene binding of α4β2* nicotinic acetylcholine receptors (nAChRs). ^{18}F-nifene uptake in the human brain was found to correspond closely with known α4β2* nAChR distributions, and test–retest variability was consistent with other neuroreceptor radioligands. Images show that the distribution volume ratio in the cerebellum was similar to that in the cortex.

potential to overcome some of the timing disadvantages of ^{18}F-fluoromisonidazole, with lower lipophilicity and easier radiosynthesis. In this study, they looked at radiation dosage, biodistribution, human safety, tolerability, and early elimination of ^{18}F activity in urine after injection of a single dose of ^{18}F-DiFA in healthy volunteers. No adverse effects were found to be associated with tracer injection, and the tracer was rapidly excreted from all organs, with an effective dose that was within the range of other common ^{18}F PET tracers. Figure 4 (top) shows biodistribution over a 1-h period after a 717.8-MBq injection, and Figure 4 (bottom) is a representative image of uptake at 1, 2, 4, and 6 hours after injection. The tracer clears the liver and is excreted by the kidneys. The authors concluded that their data "support the further application of ^{18}F-DiFA for clinical imaging of tumor hypoxia."

Another "first application" study came from Lao et al. from the University of California Irvine, the University of Pittsburgh (PA), and the University of Wisconsin–Madison, who reported on "First-in-humans PET study: biodistribution, test–retest variability, and dosimetry of the α4β2* nicotinic acetylcholine receptor (nAChR) agonist radiotracer ^{18}F-nifene" [836]. The study included 8 healthy individuals who underwent 90-minute dynamic ^{18}F-nifene PET imaging at baseline and again 58 ± 31 days later. They found that ^{18}F-nifene uptake in the human brain corresponds closely with known α4β2* nAChR distributions, and test–retest variability (<7%) was consistent with other neuroreceptor radioligands. The thalamus showed the highest distribution volume ratio in all subjects, followed by the striatum, cortical regions, temporal cortex, and parietal cortex, with fast brain kinetics and renal clearance (Fig. 5). They concluded that "^{18}F-nifene demonstrates favorable kinetics and imaging properties in humans and has promise for in vivo investigation of the nAChR system in longitudinal or drug therapy studies."

Luo et al. from Peking Union Medical College Hospital (Beijing, China) reported that "^{68}Ga-exendin-4 PET/CT is both sensitive and specific in diagnosing insulinomas" [237]. In previous investigations, this group showed that glucagon-like peptide-1 receptor imaging with this agent can be used effectively for identification of insulinomas. In this study, 164 patients with hyperinsulinism were imaged with ^{68}Ga-exendin-4 PET/CT, contrast-enhanced CT with perfusion, MR, endoscopic ultrasound, and somatostatin scintigraphy. ^{68}Ga-exendin-4 PET/CT was positive for

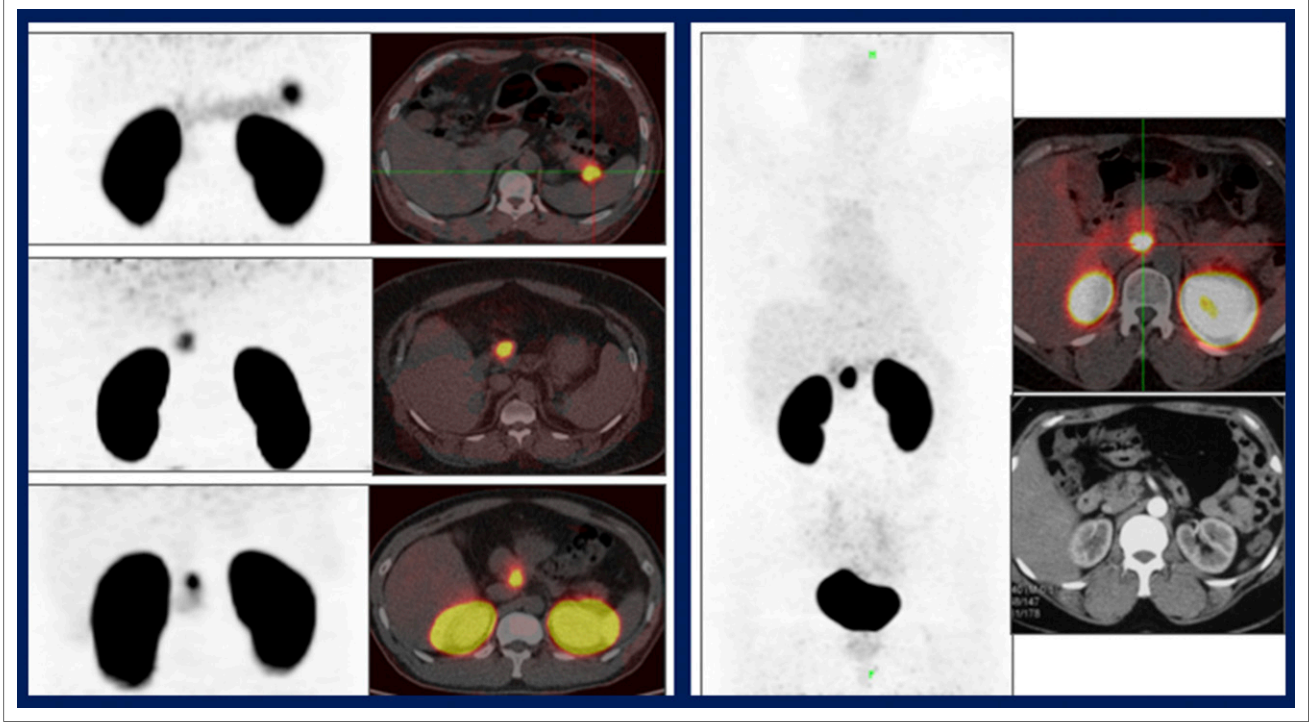

FIGURE 6. ^{68}Ga-exendin-4 PET/CT (right images in the right and left blocks) in 4 patients in whom previous surgery failed to remove insulinomas and in whom contrast-enhanced CT with perfusion, MR, endoscopic ultrasound, and somatostatin scintigraphy (left images in the right and left blocks) were negative. The sensitivity, specificity, accuracy, and positive and negative predictive values for ^{68}Ga-exendin-4 PET/CT in diagnosing insulinoma were 99.0%, 100%, 99.3%, 100%, and 98.3%, respectively. After PET identification of insulinomas, patients underwent surgical removal or ethanol ablation.

insulinoma in 110 of those patients, with 101 confirmed at surgery (the remaining 9 underwent either nonsurgical ablation or biopsy of distant metastasis). PET/CT also identified multiple lesions in a significant subset of patients. The sensitivity, specificity, accuracy, and positive and negative predictive values for ^{68}Ga-exendin-4 PET/CT in diagnosing insulinoma were 99.0%, 100%, 99.3%, 100%, and 98.3%, respectively. This is a welcome innovation—trying to locate these lesions with dynamic CT or MR is somewhat difficult. Figure 6 shows comparison imaging in 4 patients in whom CT, MR, endoscopic ultrasound, and somatostatin scintigraphy were negative but who were positive on ^{68}Ga-exendin-4 PET/CT. The delineation is clear on PET/CT—this is nuclear medicine at its best. The authors concluded that this may be developed into an accurate screening test for insulinomas in patients with hypoglycemia.

Jiang et al. from the Mayo Clinic (Rochester, MN) reported on "Current Good Manufacturing Practice (cGMP) synthesis of sodium iodide symporter (NIS) probe ^{18}F-tetrafluoroborate (^{18}F-TFB) and biodistribution in healthy male and female human subjects" [682]. ^{18}F-TFB is an iodide analogue with potential for imaging of differentiated thyroid cancer and as an NIS gene reporter probe. The authors' objectives were to develop an automated and cGMP-compatible method for synthesis of ^{18}F-TFB and to evaluate safety and biodistribution in healthy volunteers. Automated cGMP synthesis of ^{18}F-TFB via ^{18}F-fluorination of BF_3 was successful, with radiochemical yields of 32% ± 2% and specific radioactivity of 2.2 ± 0.9 GBq/mmol. The injected tracer was well tolerated, with no adverse events. Biodistribution was consistent with that of radioiodide, supporting the potential for clinical application of ^{18}F-TFB PET imaging of differentiated thyroid cancer and in NIS gene reporter studies. Figure 7 (top) shows coronal ^{18}F-TFB PET/CT images (left, CT; middle, fused; right, PET) at 2.5 h after injection in a healthy woman. Activity in the salivary glands, thyroid, stomach, and bladder excretion are clearly visible—much as in a radioiodine scan. Figure 7 (bottom) shows the same series in a healthy man. If further development shows this tracer to be effective, one clear advantage will be the ability to perform the procedure efficiently in a single day with, of course, no possibility of stunning.

O'Donoghue et al. from Memorial Sloan Kettering Cancer Center (New York, NY) and MabVax Therapeutics (San Diego, CA) reported on "Biodistribution and radiation dose estimates for ^{89}Zr-DFO-HuMab-5B1 (MVT-2163) in CA19-9–positive cancer: first-in-man results" [837]. More than 90% of pancreatic cancers are positive for the CA19-9 antibody. The investigators examined 12 patients with metastatic pancreatic cancer, each of whom received ~185 MBq of the tracer but different amounts of cold antibody (0, 17, or 47 mg). Patients underwent multiple full-body ^{89}Zr-DFO-HuMab-5B1 PET acquisitions as well

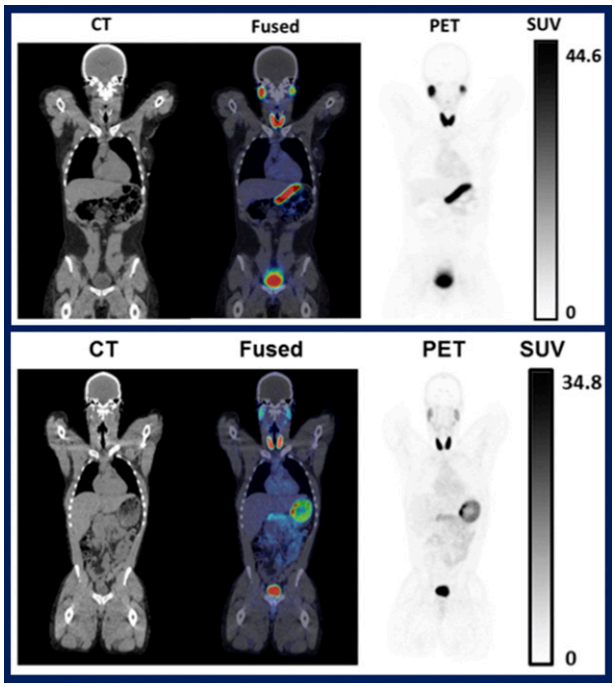

FIGURE 7. Top: Coronal ^{18}F-TFB PET/CT images (left, CT; middle, fused; right, PET) at 2.5 hours after injection in a healthy woman. Activity in the salivary glands, thyroid, stomach, and bladder excretion are clearly visible. Bottom: Corresponding images in a healthy man. ^{18}F-TFB is an iodide analogue with potential for imaging of differentiated thyroid cancer and as a sodium iodide gene reporter probe.

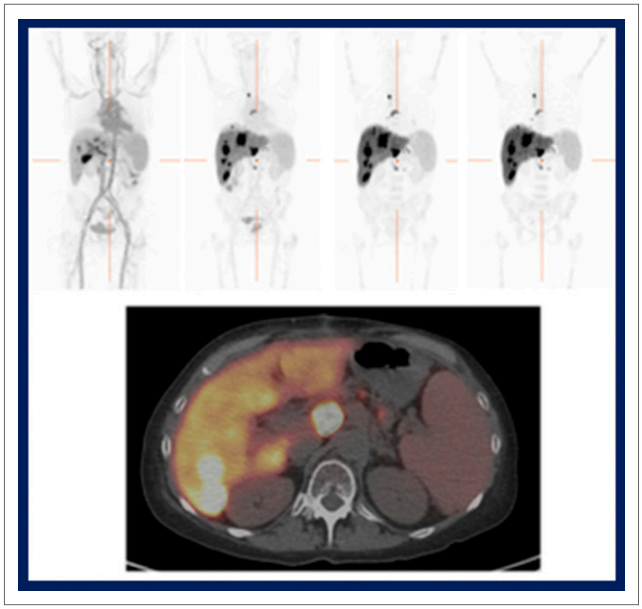

FIGURE 8. Top: Representative series of multiple intensity projection images showing a typical evolution of MVT-2163 biodistribution at (left to right) 1, 20, 44, and 141 hours after injection of ^{89}Zr-DFO-HuMab-5B1. Focal uptake was seen from early on in metastatic disease in the ilium and also in numerous small nodes in the chest/abdomen, becoming progressively more distinct with time.

as serum analysis and whole-body counts acquired using a NaI(Tl) scintillation detector during 7 days after injection. Image- and count-derived residence times were used with OLINDA/EXM to estimate normal tissue radiation doses. Clearance rates averaged around 218 hours for the whole body. Cohort comparisons showed that increasing antibody mass dose and increasing time between cold and hot administrations tended to reduce liver and spleen uptake. Figure 8 shows biodistribution in a patient over 141 hours. It is important to note the theranostic potential of agents such as this. It is very likely that this agent could be labeled with ^{177}Lu (in fact, groups are already working on this) or other therapeutic agents. Theranostic applications offer extraordinary promise for new horizons in nuclear medicine, taking us beyond diagnosis and monitoring.